ISSN: 2278 – 909X
International Journal of Advanced Research in Electronics and Communication Engineering (IJARECE)
Volume 5, Issue 5, May 2016

Design of Metamaterial Absorber for all bands from Microwave to Terahertz ranges.

Ahmed M. Montaser.

Abstract— **In this article a new kind of metamaterial absorber (MTMA) for many applications in the microwave and terahertz ranges is proposed. The suggested MTMA has simple configuration which is pliant to regulate the metamaterial (MTM) properties to be used in terahertz band and can easily be re-scaled to other bands of frequency. In microwave range, three maxima in the absorption are empirically obtained around 99% at 2.8 GHz for the first band, 99% at 4.1 GHz for second band and 89% at 5.8 GHz for third band, that result achieves a good agreement with the simulation result from both CST Microwave Studio Package and the Finite Difference Time Domain (FDTD) program written in Matlab. The proposed MTMA supplies consummate absorption for terahertz frequency ranges and can be used for the accomplishment of more efficient solar cells. As a result, the proposed MTMA and its variations in microwave range enable myriad potential applications in long distance radio telecommunications, satellite communication transmissions, some Wi-Fi devices, some cordless telephones, some weather radar systems, medical imaging, sensors and etc.**

Index Terms FDTD, Metamaterial, Terahertz, Tri-band.

I. INTRODUCTION

The metamaterials (MTMs) are artificial structures that can be designed to show specific electromagnetic (EM) properties not commonly found in nature [1-2]. The first metamaterial is fabricated in 2000 by Smith and Kroll [3] with periodically disposed inclusions composed of a split ring resonator and wire structures. MTMs provide many interesting applications, such as super lens [4], cloaking [5], and negative refraction [6], absorber [7], etc. Due to the fascinating performances, the new kind of materials can dramatically add a degree of freedom to control electromagnetic waves. As a result, the emergence of metamaterials has attracted significant attention in THz regime, where natural materials perform weak electric and magnetic response [8, 9]. The first experimental realization of THz metamaterial was reported by T. J. Yen et al. in 2004 [10]. From then on, a variety of THz metamaterial-based functional devices have been realized, including intelligent switches, sensors, modulators, absorbers and so on [11-13].
The demonstration of metamaterial perfect absorbers [14, 15] represents one of the most important applications employing the astonishing properties found in metamaterials [16]. The original idea [3] is that, in MTMAs with simultaneous electrical and magnetic resonances, both of the ineffectual permittivity ε(ω) and permeability μ(ω) are highly dispersive and can be tailored independently. However, some researchers have proposed polarization independent fishnet metamaterials [17-19]. It has also been shown that fishnet metamaterials can support multiple magnetic resonances corresponding to the excitation of different orders of SPP modes [20]; however, only up to two negative index bands (i.e., dual-band) have been demonstrated in the sub-THz [19], near-IR [21], and near-IR/visible [7] regimes. While the idea of styling a resonant absorber could be of possibility use throughout the electromagnetic spectrum, this concept is expected to be especially productive at terahertz frequencies where it is difficult to find strong absorbers. However, for the recent years, researchers have been studying MTMs for visible and infrared ranges [22, 23].
This paper focuses on artificial structures to design, characterize, and analyze a new type of MTMA wrapping the microwave and terahertz spectrum range to apply the energy effectively. The proposed design is single layered flexible design has a mechanical tunability feature. Both numerical simulation and experimental measurements are carried out in the microwave region to verify the idea to be a fundamental structure for other regimes, especially in infrared and visible frequency ranges and to be used in solar cells for improving their efficiencies. The performance is also independent of the polarization of the incidence waves. Our proposed sample, according to the simulation result, shows a strong resonance and it's all cases provide perfect absorption in corresponding microwave and terahertz ranges. In microwave range is validated by both simulation and experimental studies, the measurement results were obtained by manufacturing the proposed sample for C-band and it was shown that the measurement results achieve a good agreement with the simulation results obtained by both a software CST Microwave Studio package and the Finite Difference Time Domain (FDTD) program written in Matlab. According to the obtained results, we accept the proposed structure can be used in terahertz frequencies by change scaling its dimensions. The surface current and electric field distributions are also analyzed to explain the physical mechanism of our design. The organization of this article is as follows. In section II the simulation and experimental configuration of the metamaterial absorber design is explained. Numerical and measurement results are discussed in Section III. Finally, Section IV presents the conclusions.

Manuscript received May , 2016.
Ahmed M. Montaser, *Sohag University, Sohag, Egypt.*

ISSN: 2278 – 909X
International Journal of Advanced Research in Electronics and Communication Engineering (IJARECE)
Volume 5, Issue 5, May 2016

II. Simulation and Experimental Studies

Fig. 1 shows the schematic diagram of the implemented metamaterial unit cell for microwave range. The design unit cell is simply built of a metallic hexagonal resonator includes a centered cross mark (+) and four split-ring resonators (SRRs) distributed around the cross mark symmetrically. The radius of the metallic hexagonal resonator is 12 mm, and the structure has dimensions of L_2 = 10.5, L_3 = 1.5 mm, L_4 = 1.5 and L_5 = 8 mm, while the four SRRs have dimensions of r_1 = 2 mm, r_2 = 3 mm, and g_1 = 1 mm. The four SRRs are placed within the four quadrants formed by the cross mark with relative distance 3.5 mm from the cross edges, and the split ring gaps are oriented at right angles with respect to the adjacent edge of the cross mark, as illustrated in Fig. 1(a). The proposed MTM unit cell is built on a cheaper substrate (FR4) with relative permittivity, loss tangent and thickness are 4.2, 0.02, 1.6 mm respectively.

The metallic structures on the top and bottom planes of the substrate are chosen as copper with the electrical conductivity of 5.8×10^7 S/m. Copper is used in microwave applications. The Drude model approximation, in terahertz ranges, is used to describe the influence metallic dielectric properties of the metallization which can be given as $\varepsilon(f) = 1 - f_p^2/(jf\gamma + f^2)$, where f_p is the plasma frequency and γ is the damping rate of the material. The following values are used for the plasma frequency and damping rate: f_p = 2180 THz and γ = 4.35 THz [24, 25]. The unit cells have the following periodicities: 30mm × 30mm for microwave frequencies as shown in Figure 1(d), 2750 nm × 2750 nm with the thickness of 250 nm for infrared frequencies, and 1150 nm × 1150 nm with the thickness of 200 nm for visible frequencies.

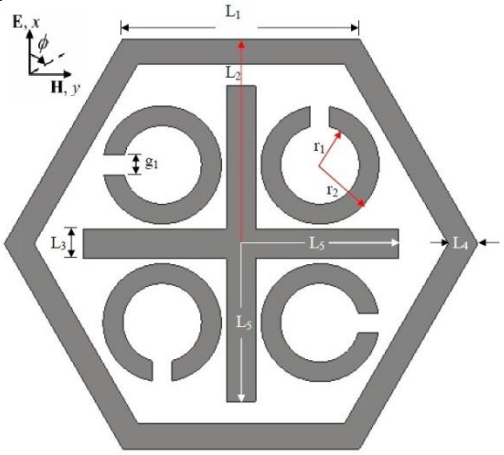

(a)

(b) (c) (d)

Fig. 1. Designed and fabricated absorbers. (a) Unit cells with dimensions. (b) Schematic of the unit cell. (c) Fabricated unit cell. (d) Fabricated structure sample.

The executions of the solitary elements in the unit cell are not consummate for the main resonance as in the united one. This means that the union of the solitary elements runs effectively together and purveys consummate absorption for the main mode. In order to obtain experimental results, the structure is optimized for microwave frequencies and then 6 × 6 unit cell periodic structure with the overall size of 324 cm^2 is fabricated as shown in Fig. 1(d).

The simulation of the periodic structure was fulfilled with a software CST Microwave Studio package based on finite integration technique (FIT). The periodic boundary conditions with floquet port is used in the simulation. In addition, the periodic structure is assessed using the Finite Difference Time Domain (FDTD) program written in MATLAB to validate the results. The measurement is carried out by using R&S ZVL6 Vector Network Analyzer (VNA) and two horn antennas. In the measurement, one horn antenna acts as a transmitter and the other one detects the transmitted or reflected wave. Firstly, free space measurement without a sample is carried out and this measurement used as the calibration data for the VNA. The sample is then incorporated into the experimental measurement setup and S-parameters measurements are performed. The sample and devices used in this experiment are shown in Fig. 2. Note that the transmitter antenna and the front side of the sample are arranged to form a face-to-face configuration with each other in the measurement.

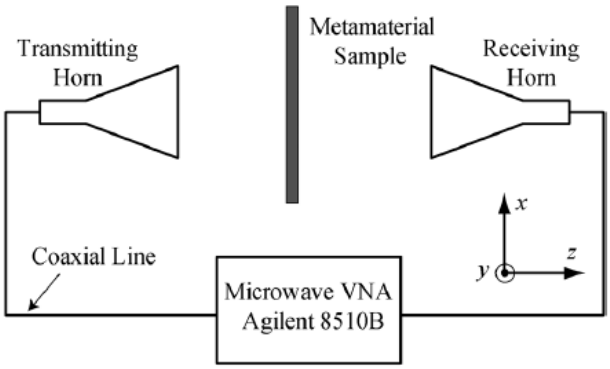

Fig. 2. Experimental setup for measuring the transmission spectrum of the metamaterial.

III. Numerical And Experiment Results

At first, the numerical study is performed for the MTMA absorber structure. After that, the results are verified by measuring the S-parameters. As cleared, the suggested structure will not have transmission because of the metallic plate located on its backside. The selected geometry provides strong absorption at a certain frequency (2.8 GHz) because of structural properties which decreases the reflection of the applied incident electromagnetic wave and can suitably be used in many applications where high absorption is required, in addition, there are a second and third absorption bands in which the reflection is also minimized.

Figures 3 and 4 show the simulation and measurement results for the reflection and absorption spectra for microwave C-band frequency range. Three different

resonances occur around 2.8 GHz, 4.1 GHz and 5.8 GHz in the reflection spectrum, thus yielding three maxima in the absorption.

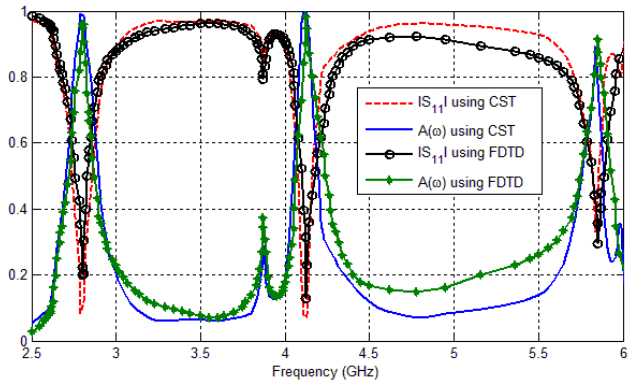

Fig. 3. Simulated return loss (S_{11}) and absorption of the suggested MTMA for microwave C-band frequency range.

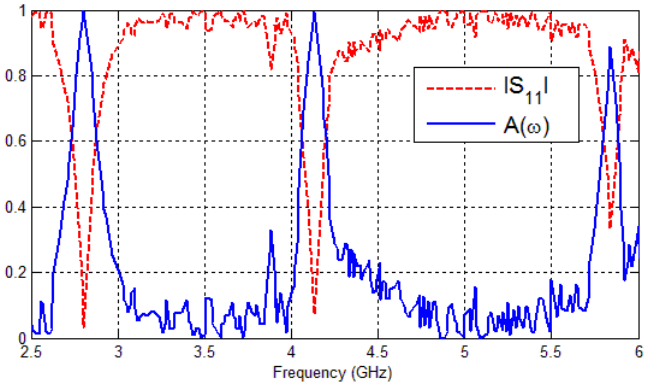

Fig. 4. Measured return loss (S_{11}) and absorption of the suggested MA for microwave C-band frequency range.

To validate the numerical results which have obtained from the CST simulator, the proposed sample has been designed by FDTD method, the FDTD program written in MATLAB. The parameters for FDTD computation were set as follows: the domain was 720 × 720 × 45 cells with a cell size of Δx = 0.25 mm, Δy = 0.25 mm, Δz = 0.125 mm and a time step of 1053.4 *fs*. For the CST Microwave Studio simulator, which based on the Finite Integration Technique (FIT), the following settings were used for time domain simulations: the minimum mesh step = 0.5, maximum mesh step = 6.852 and the mesh cells = 273,660 (N_x = 107, N_y = 119, N_z = 20). The mesh line ratio limit was set to 50 with an equilibrate mesh ratio of 1.19. Measurement setup is used for verifying numerical results, the first and second peaks are about 99% both in the simulation and experiment, and the third one is 89% in the simulation and 88% in the experiment.

The accuracy of the measurements can be clarified by the good agreement between the simulation and experimental results. For the first and second resonance, the reflection is very close to zero, which means the effective impedance $Z(\omega) = \sqrt{\mu(\omega)/\varepsilon(\omega)}$ of the medium matches with the free space impedance $Z(\omega) = Z_0(\omega) = 120\pi$ and therefore, the reflection is minimized [26-28]. This concept has been proven both numerically and experimentally in which the sample has non reflection at the first and second resonances. For the third band, perfect impedance matching is not satisfied. Thus, the structure provides three distinct absorption bands in which the first and second ones are perfect and the third one is relatively good. Therefore, the proposed model can be a good practical nominee among its counterparts operated at the same frequency region reported in literature. Furthermore, the bandwidth calculations are also performed to show the quality of the proposed absorber. So that, the fractional bandwidth (FBW) of the absorption region is computed. FBW can be found by dividing the bandwidth of the absorber to its center frequency. It can be calculated as FBW = Δf / f_0, where Δf is the half power bandwidth and f_0 is the center frequency. For the first resonance, these parameters are computed as Δf = 0.13 GHz, f_0 = 2.8 GHz and FBW ≈ 4.64% from the simulation and Δf = 0.11, f_0 = 2.8 GHz, and FBW ≈ 3.93% for the experiment. For the second resonance, the related parameters are Δf = 0.1, f_0 = 4.1 GHz, and FBW ≈ 2.44% from the simulation and Δf = 0.21, f_0 = 4.1 GHz, and FBW ≈ 5.12% from the experiment. For the third resonance, the related parameters are Δf = 0.12, f_0 = 5.84 GHz, and FBW ≈ 2.1% from the simulation and Δf = 0.24, f_0 = 5.8 GHz, and FBW ≈ 4.1% from the experiment. These computations signify that the proposed structure has good quality character [29, 30].

Moreover, we performed some simulations using the suggested structure for infrared and visible frequency ranges. For the suggested model introduces flexibility to adjust its MTMA properties, the structure is easily rescaled for THz ranges like as infrared and visible frequency bands. To validate the numerical results which have obtained from the CST simulator in terahertz regime, the proposed sample (both infrared and visible regimes) has been designed by FDTD method, the FDTD program written in MATLAB. The parameters for FDTD computation in the infrared regime were set as follows: the domain was 720 × 720 × 45 cells with a cell size of Δx = 22.9 nm, Δy = 22.9 nm, Δz = 22.9 nm and a time step of 1739 *fs*. But the parameters for FDTD computation in the visible regime were set as follows: the domain was 720 × 720 × 45 cells with a cell size of Δx = 11.25 nm, Δy = 11.25 nm, Δz = 11.25 nm and a time step of 1924 *fs*. For the CST Microwave Studio simulator, which based on the Finite Integration Technique (FIT), the following settings were used for time domain simulations in infrared regime: the minimum mesh step = 0.152, maximum mesh step = 4.61 and the mesh cells = 471, 541 (N_x = 161, N_y = 139, N_z = 21). But the parameters for CST Microwave Studio simulator invisible regime: the minimum mesh step = 0.135, maximum mesh step = 3.94 and the mesh cells = 567, 257 (N_x = 176, N_y = 142, N_z = 23). The mesh line ratio limit was set to 50 with an equilibrate mesh ratio of 1.19. Also, it is found that, there are some differences between the results of EM Simulation and that produced from the FDTD program written in MATLAB due to the different applied numerical techniques (FDTD and FIT). Maximum absorptions for infrared and visible ranges are numerically obtained around 99.46% at 265.8 THz and 99.4% at 556.4 THz as shown in Figs 5 and 6, respectively.

The influences of the polarization angle on the conduct of the suggested metamaterial absorber are tested for microwave frequency range. The frequency response of the absorption behavior can be seen in Fig. 7. The polarization

angle φ is distinct as the angle between electric field (E) and x-axis as shown in the inset in Fig. 1(a). Due to the fourfold rotational of the geometry, the magnitude and frequency of the peak absorption are both nearly invariant as the φ increases from 0^o to 90^o. Therefore, the proposed metamaterial absorber is insensitive to the polarization angle of the normal incident wave. It continues to provide the same feature for all angles at the first, second and third resonance with very small shift.

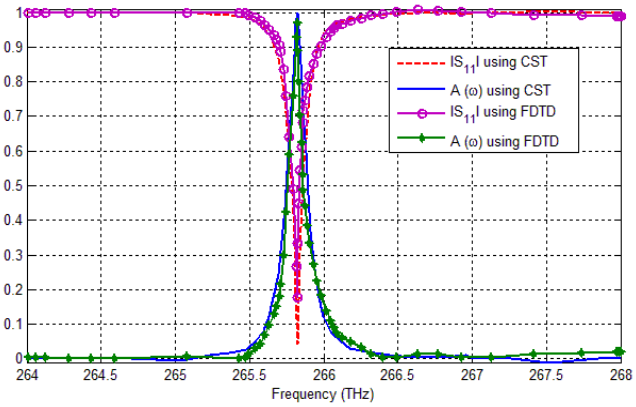

Fig. 5. Simulated return loss (S_{11}) and absorption in the infrared region.

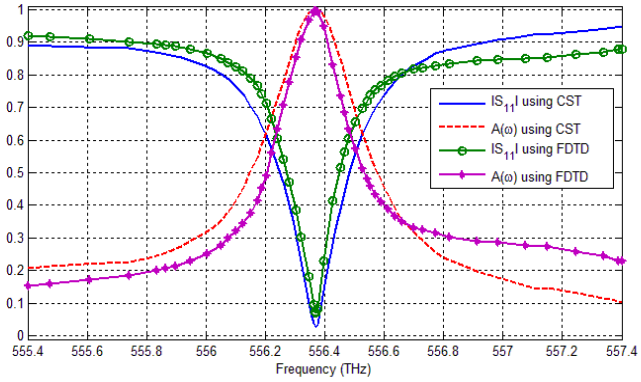

Fig. 6. Simulated return loss (S_{11}) and absorption in the visible region.

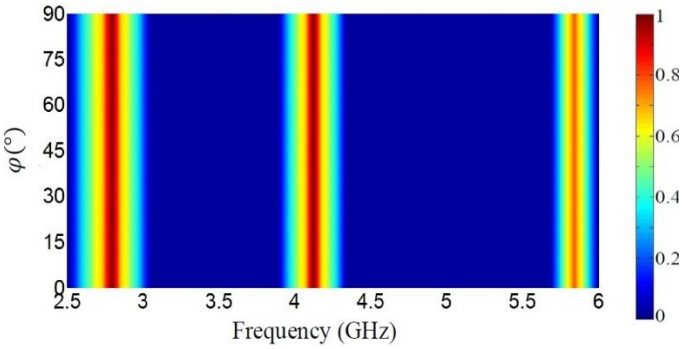

Fig. 7. Simulated absorption for various polarization angles for the normal incidence.

To better understand the mechanism of the proposed metamaterial absorber at the resonances, the electric field and surface current distributions are illustrated at the resonant frequencies and the results are shown in Figures 8, 9. In Figure 8, for f = 2.8 GHz, high concentration of the electric field around the corner of hexagonal resonator, terminals of cross mark metal and some parts from SRRs, in order, is observed. The surface charges are activated with an electric field and create magnetic response and resonant absorption. These currents are excited by magnetic and electric field coupling and persuade magnetic and electric field responses to couple with the externally applied field. It was observed that there is circulating and parallel currents in the pattern, the circulating currents are responsible for the magnetic response while the parallel currents are in charge of the electric response. Thus, the mentioned currents are driven by strong magnetic and electric coupling. They induce magnetic and electric responses which can strongly couple with the harmonizing field of the incident EM wave. Thus, strong localized EM field enhancement is established at the resonance frequency. It demonstrates that electric and magnetic resonances appear at this resonant frequency simultaneously, which provide the ability to absorb the electromagnetic radiation almost completely under the matching condition ($Z(\omega) = Z_0(\omega)$). Therefore, whole incident energy is confined in the absorber that means reflection is minimized on the contrary of absorption. Thus, EM energy is confined in the structure, which yields near zero reflection and unity absorption. While the second resonance, which is located at 4.1 GHz as shown in Figs. 8 and 9. The electric field is concentrated on the arms of the cross mark metal and some part of SRRs ring, the electric and magnetic resonances appear at this resonant frequency too as before. Furthermore, different observations are also monitored for the third resonance located at 5.8 GHz expects its mode as shown in Figs. 8 and 9. However, this mode is not stronger as in the previous resonances thus the third reasonable absorption compared to the previous resonances. Note that it averagely provides 89% absorption, although it is relatively weaker than first or second resonance.

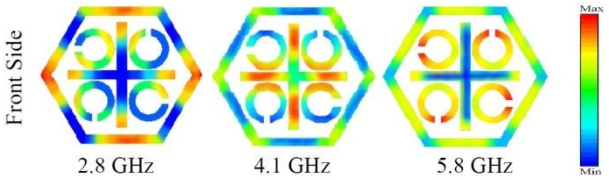

Fig. 8. Electric field distributions at the resonant frequencies of one cell for microwave frequency region.

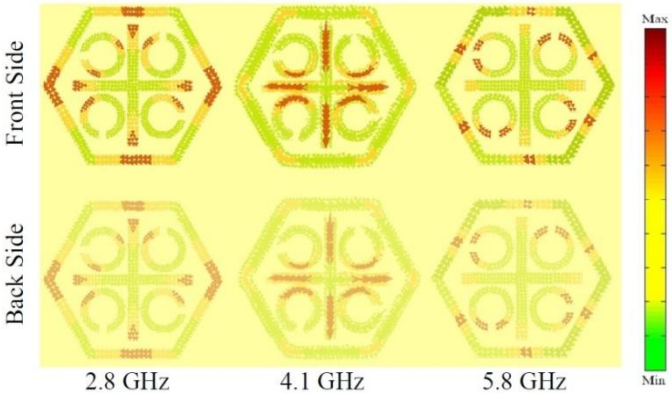

Fig. 9. Surface current distributions at the resonant frequencies of one cell for microwave frequency region.

The results present that the absorber has nearly no polarization dependency for the all resonances for the any arbitrary polarization with a wide range of incident angles.

Consequently, the proposed design can be used as a perfect absorber with the capability of wide-angle incidence and polarization independency, which is very useful for the medical applications such as medical imaging, for different polarizations and different angles provide nearly same absorption character. Therefore, the suggested structure can be used in long-distance radio telecommunications (as directly related with Microwave band) and it will be a very good nominee for the applications of some Wi-Fi devices, satellite communication transmissions, some weather radar systems and some cordless telephones.

Moreover, the influences of the polarization angle on the conduct of the terahertz-frequency samples are significant and it is tested both for infrared and visible frequency ranges. The frequency response of the absorption conduct can be shown in Fig. 10.

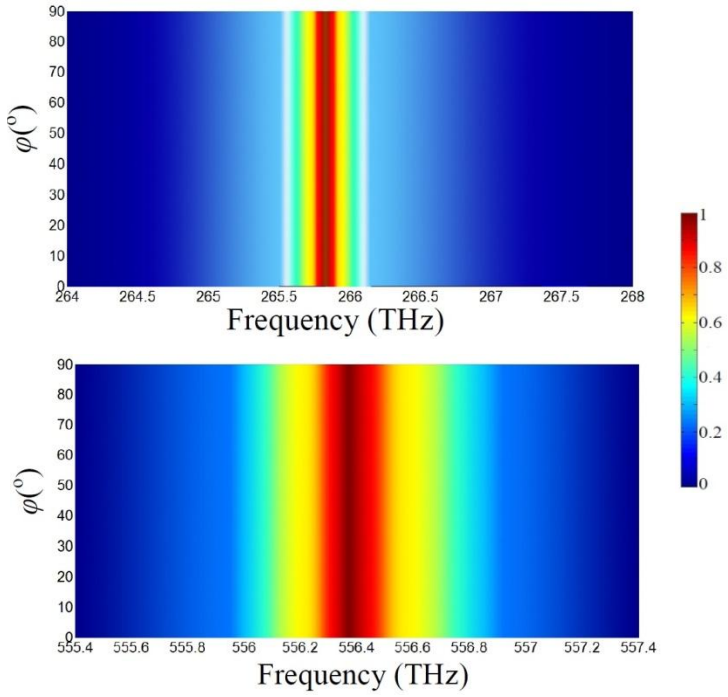

Fig.10. Simulated results of the absorbing execution under various polarization angles for terahertz frequency ranges.

It can be distinctly observed, there are very small frequency shifts relying on the angle changes and these shifts are in the trivial level. The absorption levels are not influenced from the polarization angle variations and the same conducts are noticed as the microwave structure (contrasting with result of Fig. 7). This drives at no annexation components are required to have a high-level absorption with polarization angle independence. If this structure used for solar cell applications, this will provide a great advantage for the solar cell system since the incident waves will change constantly during the day. With this behavior the structure will remain in the same position and no additional control units would be necessary. Briefly, the solar system would receive the maximum level of light absorption during all day when the proposed MA is implemented into the system. Also, as fixed, the proposed structure provides forceful absorption at a particular frequency because of the structural properties which minimizes the reflection for the applied incident EM wave. This is significant for solar cell systems for more solar energy will be produced when the consummate absorption is acquired.

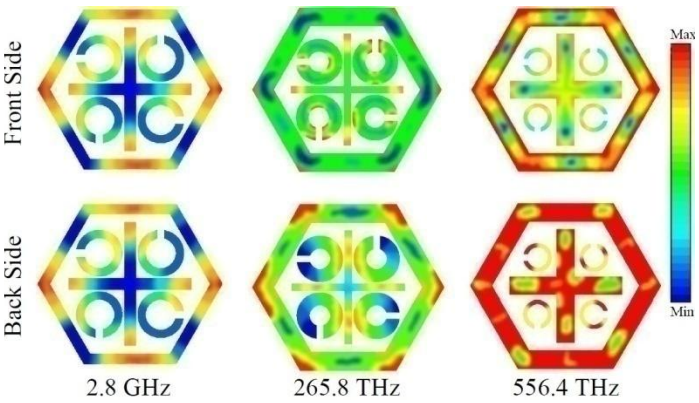

Fig. 11. Electric field distributions at the resonant frequencies of one cell for microwave and terahertz frequency regions.

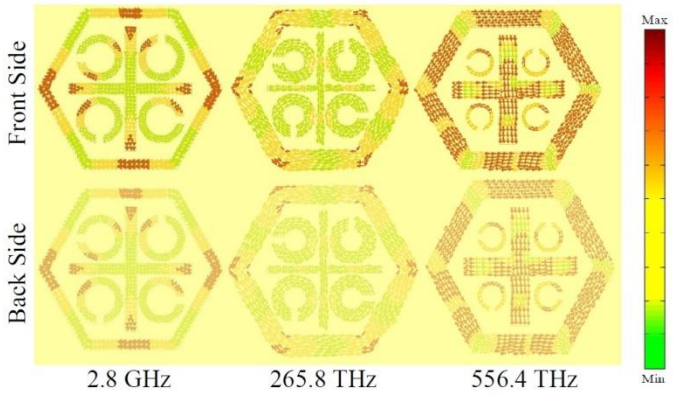

Fig. 12. Surface current distributions at the resonant frequencies of one cell for microwave and terahertz frequency regions.

With a view to explain the corporeal mechanism of the electric field and surface current distributions in terahertz ranges on MTMA at the resonances, the electric field and surface current distributions are studied at the resonant frequencies and the results can be seen in Figs 11, 12. In Figure 11, the microwave frequency f = 2.8 GHz has been explained previously. The electric field distribution for the second resonance frequency f = 265.8 THz, which is shown in the midsection of Fig. 11, is condensed mainly just about the edges of hexagonal for both front and back sides, the electric field strongly couples with both sides of the overall structure and induces free electric response, and the corresponding current distribution in the midsection of Fig. 12 is congruently distributed. In other words, at this frequency point, electric and magnetic resonances are also happening. Even though the absorbance level is consummate at this band, the performer of the mode is different than the others. Resembling corporeal mechanisms are effective for this resonance too. On the right side of Fig. 11, third resonance, one can observe that the electric field distribution is condensed at the edges of the front-side of the structure and there is a mighty electric field at the back side of the structure. Currents heap up at around the edges for both horizontal and vertical sections. Mighty piling up of the currents causes an electric resonance and the current currency waives a magnetic response. Thus, an absorption conduct can be noticed.

IV. Conclusion

A triple-band microwave absorber had been designed and fabricated. Moreover, high frequency MTMAs are designed and simulated at terahertz bands. The suggested absorber appears influential results for microwave band and it is easily rescaled for higher ranges of frequency for several applications. The empirical results are in a good compatibility with the simulated ones in the microwave band. Both the simulated and measured absorption values are kept around unity (~ 99%) almost for all resonances. It means that the execution of the plain structure is quite good for varied regions of the EM spectrum wraps wide range of frequencies. The bandwidth and quality factor of the absorber are relatively good with respect to its counterparts. Furthermore, it is proved that the MTMA has polarization angle independency in all frequency bands which is significant for many applications. Beyond, the electric field and surface current distributions are presented and analyzed to comprehend the resonance absorption mechanism. As a result of the above, the proposed MTMA capable of adopted to several frequency bands for various applications for instance solar cells systems, satellite communication transmissions, medical imaging, etc.

Acknowledgement

We would like to acknowledge the Electronics Research Institute (ERI), Microstrip Department for the support, encouragement, help and cooperation during simulation of this research.

References

[1] Dong, J. F., "Surface wave modes in chiral negative refraction grounded slab waveguides," Progress In Electromagnetics Research, Vol. 95, pp. 153-166, 2009.

[2] Burlak, G., "Spectrum of Cherenkov radiation in dispersive metamaterials with negative refraction index," Progress In Electromagnetics Research, Vol. 132, pp. 149-158, 2012.

[3] Smith, D. R. and N. Kroll, "Negative refraction index in left handed materials," Phys. Rev. Lett., Vol. 85. pp. 2933-2936, 2000.

[4] Fang, N., H. Lee, C. Sun, and X. Zhang, "Sub-diffraction-limited optical imaging with a silver superlens," Science, Vol. 308, pp. 534- 537, 2005.

[5] Pendry, J. B., D. Schurig, and D. R. Smith, "Controlling electromagnetic fields," Science, Vol. 312, pp. 1780-1782, 2006.

[6] Shelby, R. A., D. R. Smith, and S. Schultz, "Experimental verification of a negative index of refraction," Science, Vol. 292, pp. 77-79, 2001.

[7] Tao, H., N. I. Landy, C. M. Bingham, X. Zhang, R. D. Averitt, and W. J. Padilla, "A metamaterial absorber for the terahertz regime: Design, fabrication and characterization," Opt. Express, Vol. 16, No. 10, pp. 7181-7188, 2008.

[8] Chen, H.-T., W. J. Padilla, M. J. Cich, A. K. Azad, R. D. Averitt, and A. J. Taylor, "A metamaterial solid-state terahertz phase modulator," Nature Photonics, Vol. 3, pp. 148-151, 2009.

[9] Han, J., A. Lakhtakia, and C.-W. Qiu, "Terahertz metamaterial with semiconductor split-ring resonators for magnetostatic tenability," Opt. Express, Vol. 16, No. 19, pp. 14390-14396, 2008.

[10] Yen, T. J., W. J. Padilla, N. Fang, D. C. Vier, D. R. Smith, J. B. Pendry, D. N. Basov, and X. Zhang, "Terahertz magnetic response from artificial materials," Science, Vol. 303, No. 5663, pp. 1494-1496, 2004.

[11] Chen, H.-T., W. J. Padilla, J. M. O. Zide, A. C. Gossard, A. J. Taylor, and R. D. Averitt, "Active terahertz metamaterial devices," Nature, Vol. 444, No. 7119, pp. 597-600, Nov. 2006.

[12] Christian, D. and H. B. Peter, "Frequecncy selective surfaces for high sensitivity terahertz sensing," App. Phys. Lett., Vol. 91, No. 18, pp. 184102(1)-184102(3), Aug. 2007.

[13] A. Al`u, F. Bilotti, N. Engheta, and L. Vegni, "A thin absorbing screen using metamaterial complementary pairs," in Proceedings of the International Conference on Electromagnetics in Advanced Applications, (Turin, Italy, September 12-16, 2005), pp. 75–78.

[14] N. I. Landy, S. Sajuyigbe, J. J. Mock, D. R. Smith, and W. J. Padilla, "Perfect metamaterial absorber," Phys. Rev. Lett. 100, 207402 (2008).

[15] H.-T. Chen, J. F. O'Hara, A. K. Azad, and A. J. Taylor, "Manipulation of terahertz radiation using metamaterials," Laser Photon. Rev. 5, pp. 513–533 (2011).

[16] C. García-Meca, J. Hurtado, J. Martí, A. Martínez, W. Dickson, and A. V. Zayats, "Low-loss multilayered metamaterial exhibiting a negative index of refraction at visible wavelengths," Physical Review Letters, vol. 106, p. 067402, 2011.

[17] P. Ding, E. J. Liang, W. Q. Hu, L. Zhang, Q. Zhou, and Q. Z. Xue, "Numerical simulations of terahertz double-negative metamaterial with isotropic-like fishnet structure," Photonics and Nanostructures - Fundamentals and Applications, vol. 7, pp. 92-100, 2009.

[18] C. Sabah and H. G. Roskos, "Dual-band polarization-independent sub-terahertz fishnet metamaterial," Current Applied Physics, vol. 12, pp. 443-450, 2012.

[19] R. Ortuño, C. García-Meca, F. J. Rodríguez-Fortuño, J. Martí, and A. Martínez, "Role of surface plasmon polaritons on optical transmission through double layer metallic hole arrays," Physical Review B, vol. 79, p. 075425, 2009.

[20] D.-H. Kwon, D. H. Werner, A. V. Kildishev, and V. M. Shalaev, "Near-infrared metamaterials with dual-band negative-index characteristics," Opt. Express, vol. 15, pp. 1647-1652, 2007.

[21] U. K. Chettiar, A. V. Kildishev, H.-K. Yuan, W. Cai, S. Xiao, V. P. Drachev, and V. M. Shalaev, "Dual-band negative index metamaterial: double negative at 813 nm and single negative at 772 nm," Optics Letters, vol. 32, pp. 1671-1673, 2007.

[22] Liu, X., T. Tyler, T. Starr, A. F. Starr, N. M. Jokerst, and W. J. Padilla, "Taming the blackbody with infrared metamaterials as selective thermal emitters," Phys. Rev. Lett., Vol. 107, No. 4, 0459014, 2011.

[23] Lin, C. H., R. L. Chern, and H. Y. Lin, "Polarization-independent broad-band nearly perfect

absorbers in the visible regime," Opt. Express, Vol. 19, No. 2, pp. 415-424, 2011.

[24] Johnson, P. B. and R. W. Christy, "Optical constants of the noble metals," Phys. Rev. B, Vol. 6, No. 12, pp. 4370-4379, 1972.

[25] Ordal, M. A., L. L. Long, R. J. Bell, S. E. Bell, R. R. Bell, R. W. Alexander, Jr., and C. A. Ward, "Optical properties of the metals Al, Co, Cu, Au, Fe, Pb, Ni, Pd, Pt, Ag, Ti, and Win the infrared and farinfrared," Appl. Optics, Vol. 22, No. 7, pp. 1099-1119, 1983.

[26] Huang, Y. J., G. J. Wen, J. Li, W. R. Zhu, P. Wang, and Y. H. Sun, "Wide-angle and polarization independent metamaterial absorber based on snowflake-shaped configuration," Journal of Electromagnetic Waves and Applications, Vol. 27, No. 5, 552-559, 2013.

[27] Li, M. H., H. L. Yang, and X. W. Hou, "Perfect metamaterial absorber with dual bands," Progress In Electromagnetics Research, Vol. 108, pp. 37-49, 2010.

[28] He, X. J., Y. Wang, J. M. Wang, and T. L. Gui, "Dual-band terahertz metamaterial absorber with polarization insensitivity and wide incident angle," Progress In Electromagnetics Research, Vol. 115, pp. 381-397, 2011.

[29] Alici, K. B. and E. Ozbay, "Theoretical study and experimental realization of a low-loss metamaterial operating at the millimeter wave regime: Demonstrations of flat- and prism-shaped samples," IEEE Journal of Selected Topics in Quantum Electronics, Vol. 16, pp. 386-393, 2010.

[30] Ziolkowski, R. W., "Metamaterial-based source and scattering enhancements: From microwave to optical frequencies," Opto-Electronics Review, Vol. 14, pp. 167-177, 2006.

Ahmed M. Montaser was born in Luxor, Egypt in August 1981. He received his B.S. and M.S. in Communications and Electronics Engineering from South Valley University – Aswan (Egypt) in 2003 and 2009, respectively. His Ph.D. from Mansoura University, Egypt in 2013. Currently, he is an Assistant Professor at the Department of Communication and Electronics in Sohag University, Sohag, Egypt. He has served as an Editor/Reviewer of many international journals. His current research interests include the areas of antenna design, multiband PIFA antenna for mobile phone communications, computational electromagnetic, body centric wireless communications, mm-wave antennas and multiple antennas- user interactions.